UC Davis

UC Davis Previously Published Works

Title

Extended wall-adapting local eddy-viscosity model for the large-eddy simulations of multiscale flows

Permalink

https://escholarship.org/uc/item/09k1r97j

Journal

Physics of Fluids, 34(5)

ISSN

1070-6631

Authors

Dai, Shaoshi
Tang, Dan
Younis, Bassam A

Publication Date

2022-05-01

DOI

10.1063/5.0088656

Copyright Information

This work is made available under the terms of a Creative Commons Attribution License, availalbe at https://creativecommons.org/licenses/by/4.0/

Peer reviewed

eScholarship.org Powered by the California Digital Library
University of California

Physics of Fluids

Extended wall-adapting local eddy-viscosity model for the large-eddy simulations of multiscale flows

Cite as: Phys. Fluids **34**, 055117 (2022); https://doi.org/10.1063/5.0088656
Submitted: 19 February 2022 • Accepted: 28 April 2022 • Accepted Manuscript Online: 28 April 2022 • Published Online: 17 May 2022

Shaoshi Dai (戴绍仕), Dan Tang (唐聃) and Bassam A. Younis

View Online Export Citation CrossMark

ARTICLES YOU MAY BE INTERESTED IN

A flight test based deep learning method for transition heat flux prediction in hypersonic flow
Physics of Fluids **34**, 054106 (2022); https://doi.org/10.1063/5.0093438

Transitional flow structures in heated hypersonic boundary layers
Physics of Fluids **34**, 054114 (2022); https://doi.org/10.1063/5.0091192

Direct numerical simulation of film boiling on a horizontal periodic surface in three dimensions using front tracking
Physics of Fluids **34**, 052117 (2022); https://doi.org/10.1063/5.0086726

AIP Publishing

© 2022 Author(s).

Physics of Fluids ARTICLE scitation.org/journal/phf

Extended wall-adapting local eddy-viscosity model for the large-eddy simulations of multiscale flows

Cite as: Phys. Fluids **34**, 055117 (2022); doi: 10.1063/5.0088656
Submitted: 19 February 2022 · Accepted: 28 April 2022 ·
Published Online: 17 May 2022

View Online Export Citation CrossMark

Shaoshi Dai (戴绍仕),[1,a)] Dan Tang (唐聃),[1] and Bassam A. Younis[2]

AFFILIATIONS

[1]Deepwater Engineering Research Center, Harbin Engineering University, Harbin 150001, China
[2]Department of Civil and Environmental Engineering, University of California, Davis, California 95616, USA

[a)]Author to whom correspondence should be addressed: daishaoshi@163.com

ABSTRACT

We report on progress made in improving the performance of the well-established wall-adapting local eddy-viscosity model in an important class of multiscale flows, namely, that of unsteady, massively separated flows at high Reynolds number. While this model succeeds in capturing the asymptotic near-wall behavior of the eddy viscosity that enters the formulation of the model for the sub-grid scale correlations, its performance in these flows has proved to be unsatisfactory due to high levels of dissipation leading to poor predictions in the separated wakes. We have sought to improve the performance of this model by combining it with another, the regularized variational multiscale model, which better represents the interactions that occur in multiscale flows. This combination, which was implemented in OpenFOAM, was validated against experimental data for the challenging case of vortex shedding from circular cylinders at the high Reynolds number. Distinct improvements over the original model were obtained.

Published under an exclusive license by AIP Publishing. https://doi.org/10.1063/5.0088656

NOMENCLATURE

A	Projected area
C_d, C_l	Drag and lift coefficients
$\langle C_d \rangle$	Mean drag coefficient $\left(=\frac{\langle F_d \rangle}{0.5\rho U^2 A}\right)$
C'_d	Fluctuating drag coefficient $\left(=\frac{\sqrt{\sum (F_d - \langle F_d \rangle)/N}}{0.5\rho U^2 A}\right)$
C'_l	Fluctuating lift coefficient $\left(=\frac{\sqrt{\sum (F_l - \langle F_l \rangle)/N}}{0.5\rho U^2 A}\right)$
C_p	Mean pressure coefficient
C'_p	Fluctuating pressure coefficient
C_s	Smagorinsky coefficient
C_w	WALE model coefficient
D	Diameter of cylinder
E_{vv}	Power spectrum of transverse velocity
F_d, F_l	Instantaneous drag and lift forces
$\langle F_d \rangle$	Mean drag force
$\langle F_l \rangle$	Mean lift force
f_{vs}	Strouhal frequency $(= St \cdot U/D)$
$f(x)$	One dimensional function
$\bar{f}(x)$	Filtered one dimensional function
$\bar{g}_{ij}$	Velocity gradient tensor
I	Identity operator
p	Pressure
$\bar{p}$	Filtered pressure
Re	Reynolds number $(= UD/\nu)$
$\lvert\bar{S}\rvert$	Magnitude of the strain rate
$\bar{S}_{ij}$	Filtered strain rate tensor
S^d_{ij}	Traceless symmetric part of the square of the velocity gradient tensor
$\tilde{S}^s_{ij}$	Strain ratio tensor in the HPF field
$\tilde{S}^{sd}_{ij}$	Deviatoric part of the tensor in the HPF field
St	Strouhal number $(= f_{vs}D/U)$
t^*	Non-dimensional time
U	Velocity of incident flow
$\bar{u}$	Filtered velocity field
$\bar{u}'$	Fluctuations of filtered streamwise velocity
$\tilde{u}$	High-pass filtered (HPF) velocity field
$\bar{\tilde{u}}$	Low-pass filtered velocity field
$\langle \bar{u} \rangle$	Mean streamwise velocity
u_i	Velocity components

Published under an exclusive license by AIP Publishing

$\boldsymbol{u}_\tau$	Friction velocity
$\langle \bar{u}'\bar{u}' \rangle$	Mean streamwise Reynolds stress
$\overline{\bar{u}_i\bar{u}_j}$	Filtered Reynolds-stress tensor
$\bar{v}$	Filtered transverse velocity
$\bar{v}'$	Fluctuating of filtered transverse velocity
$\langle \bar{v} \rangle$	Mean filtered transverse velocity
$\langle \bar{v}'\bar{v}' \rangle$	Mean transverse Reynolds stress
y^+	Dimensionless near wall distance
$\Delta_x, \Delta_y, \Delta_z$	Grid spacing

Greek

Δ	Sub-grid characteristic length scale
δ_{ij}	The Kronecker delta
θ	Circumferential angle
ν	Kinematic viscosity
ν_{SGS}	Sub-grid eddy viscosity
ν^{w}_{SGS}	Sub-grid eddy viscosity of the WALE model
ν^{sw}_{SGS}	Sub-grid eddy viscosity of the extended model
ρ	Fluid density
τ_{ij}	Sub-grid stress tensor
$\tilde{\tau}^{s}_{ij}$	Sub-grid stress tensor in the HPF field
$\tilde{\tau}^{sw}_{ij}$	Sub-grid stress tensor of the extended WALE model
$\bar{\Omega}_{ij}$	Anti-symmetric part of velocity gradient tensor

Subscripts

i, j, k	Cartesian tensor indices
n	Filtering order

I. INTRODUCTION

While the use of large-eddy simulations (LES) has become routine in engineering calculations, certain shortcomings in their performance have persisted over time. Chief among these is the behavior, in the proximity of a solid surface, of the eddy viscosity that enters the formulation of the sub-grid scale model. The problem is well known: the eddy viscosity is assumed to be proportional to characteristic velocity and length scales of turbulence with the former deduced from the local, filtered rate of strain. This formulation invariably leads to overestimation of the eddy viscosity, especially for the flows dominated by multiscale vortex motion, since the turbulent fluctuations whose magnitude in the direction vertical to the wall are damped by its presence, thereby modifying the characteristic velocity scales to an extent that is not represented by the rates of strain there (Kobayashi,[1] Chang *et al.*[2]). In order to remedy this defect, a number of alternative modifications to the standard sub-grid scale model of Smagorinsky[3] (SM) have been reported in the literature. The particular modification that is of relevance to this work is the one by Nicoud and Ducros[4] whose wall-adapting local eddy-viscosity (WALE) model, which is based on the square of the velocity gradient tensor, has produced the correct asymptotic behavior of the eddy viscosity leading to improved predictions in a number of wall-bounded flows. The authors did, however, caution that their model 'needs to be tested in more complex cases' in order to determine its validity in flows other than the ones used in its formulation. This provided the motivation for the present work, namely, to check the WALE model's performance for high Reynolds number flows over a circular cylinder. This is a challenging flow being characterized by the occurrence of vortex shedding leading to complex interactions between the organized large-scale mean-flow periodicity and the random small-scale turbulent motions. The results were not encouraging. The solutions we obtained exhibited the over-dissipative behavior observed in other vortical flows (Modirkhazeni *et al.*,[5] Liu *et al.*[6]). The problem of excessive dissipation was addressed by Hughes *et al.*[7] who proposed the variational multiscale model (VMM) to differentiate between the large and small scales. Subsequently, a "regularized" version of this model, proposed by Winckelmans and Jeanmart,[8] was shown by Kassinos *et al.*[9] to lead to improvements in the prediction of vortical flows. However, the asymptotic near-wall behavior was not correctly reproduced (Jeanmart and Winckelmans[10]). Recently, the method of dynamically determining the model coefficients has attracted much attention to overcome problem of excessive dissipation. Examples here include the explicit algebraic sub-grid scale model of Montecchia *et al.*,[11] the Lagrangian dynamic model LDM of Tellez-Alvarez *et al.*,[12] and the dynamic k-equation sub-grid scale (SGS) model of Shukla and Dewan[13] and Sircar *et al.*[14] In many of these methods, the computational effort increases significantly due to the introduction of additional equations and test-filtering operations (Zahiri and Roohi[15]), which adversely impacts their utility for the simulation of turbulent flows around complex geometries (Gonzalez-Trejo *et al.*[16]).

In this study, we have sought to determine whether improvements in the prediction of vortex shedding from circular cylinders, an important problem due to its complex physics and its occurrence in many applications of practical interest, can be obtained by combining the WALE and the regularized variational model (RVM) approaches in order to, at once, capture the multiscale effects that dominate unsteady, massively separated flows while capturing the proper asymptotic near-wall behavior. Details of the new formulation are presented in Sec. II. The results are presented in Sec. III where comparisons are made with experimental data as well as with simulations with the standard and the dynamic K-eqn LES models. Conclusions are presented in Sec. IV. Details of the model implementation in OpenFOAM are included in the Appendix.

II. MATHEMATICAL FORMULATION

A. Governing equations

By assuming incompressible flow of a constant-property fluid, the filtered continuity and Navier–Stokes equations are

$$\frac{\partial \bar{u}_i}{\partial x_i} = 0, \tag{1}$$

$$\frac{\partial \bar{u}_i}{\partial t} + \frac{\partial \bar{u}_i \bar{u}_j}{\partial x_j} = -\frac{1}{\rho}\frac{\partial \bar{p}}{\partial x_i} + \nu \frac{\partial^2 \bar{u}_i}{\partial x_j \partial x_j} + \frac{\partial \tau_{ij}}{\partial x_j}, \tag{2}$$

where $\bar{\boldsymbol{u}}$ and $\bar{p}$ are the filtered velocity vector and pressure, respectively, τ_{ij} is the sub-grid stress, ρ is the density, and ν is the kinematic viscosity.

The sub-grid scale (SGS) model needed to approximate the values of τ_{ij} is based on the Smagorinsky assumption of a linear stress–strain relationship,[3]

$$\tau_{ij} = -(\overline{\bar{u}_i\bar{u}_j} - \bar{u}_i\bar{u}_j) = 2\nu_{\mathrm{SGS}}\bar{S}_{ij}, \tag{3}$$

$$\nu_{\mathrm{SGS}} = (C_s\Delta)^2|\bar{\boldsymbol{S}}|, \tag{4}$$

where ν_{SGS} is the sub-grid eddy viscosity, $\bar{S}_{ij}$ is the filtered strain rate tensor for the resolved scales, $\bar{S}_{ij} = \frac{1}{2}\left(\frac{\partial \bar{u}_i}{\partial x_j} + \frac{\partial \bar{u}_j}{\partial x_i}\right)$, C_s is the Smagorinsky

Published under an exclusive license by AIP Publishing

coefficient, Δ is the sub-grid characteristic length scale, which is related to the local mesh sizes $(\Delta_x\Delta_y\Delta_z)^{1/3}$, and $|\bar{S}| = (2\bar{S}_{ij}\bar{S}_{ij})^{1/2}$.

B. Model development

Nicoud and Ducros[4] put forward a proposal for improving the near-wall behavior of the standard SGS model. In this proposal, which they named the wall adapting local eddy-viscosity (WALE) model, use is made of the traceless symmetric part of the square of the velocity gradient tensor ($\bar{g}_{ij} = \frac{\partial \bar{u}_i}{\partial x_j}$), which is given as

$$S_{ij}^d = \frac{1}{2}(\bar{g}_{ij}^2 + \bar{g}_{ji}^2) - \frac{1}{3}\delta_{ij}\bar{g}_{kk}^2, \tag{5}$$

where $\bar{g}_{ij}^2 = \bar{g}_{ik}\bar{g}_{kj}$ and δ_{ij} is the Kronecker symbol.

The anti-symmetric part of $\bar{\boldsymbol{g}}$ is written as

$$\bar{\boldsymbol{\Omega}}_{ij} = \frac{1}{2}\left(\frac{\partial \bar{u}_i}{\partial x_j} - \frac{\partial \bar{u}_j}{\partial x_i}\right).$$

The tensor defined by Eq. (5) can be rewritten in terms of $\bar{\boldsymbol{S}}$ and $\bar{\boldsymbol{\Omega}}$

$$S_{ij}^d = \bar{S}_{ik}\bar{S}_{kj} + \bar{\Omega}_{ik}\bar{\Omega}_{kj} - \frac{1}{3}\delta_{ij}(\bar{S}_{mn}\bar{S}_{mn} - \bar{\Omega}_{mn}\bar{\Omega}_{mn}).$$

According to the Cayley–Hamilton theorem, the quantity $S_{ij}^d S_{ij}^d$ can be written as

$$S_{ij}^d S_{ij}^d = \frac{1}{6}(\boldsymbol{S}^2\boldsymbol{S}^2 + \boldsymbol{\Omega}^2\boldsymbol{\Omega}^2) + \frac{2}{3}\boldsymbol{S}^2\boldsymbol{\Omega}^2 + 2\boldsymbol{IV}_{S\Omega},$$

where $\boldsymbol{S}^2 = \bar{S}_{ij}\bar{S}_{ij}$, $\boldsymbol{\Omega}^2 = \bar{\Omega}_{ij}\bar{\Omega}_{ij}$, and $\boldsymbol{IV}_{S\Omega} = \bar{S}_{ik}\bar{S}_{kj}\bar{\Omega}_{jl}\bar{\Omega}_{li}$.

Depending on the value of $S_{ij}^d S_{ij}^d$, the turbulence structures can be associated with either high strain rates, high rotation rates, or both. Thus, defining a spatial operator $\overline{OP}$ to replace $|\bar{S}|$ in Eq. (4), $\overline{OP}$ will behave like y^+ near a wall, at the same time by scaling it must be of O (1) near a wall before it being used in the sub-grid scale model formulation. This has the effect of eliminating the numerical instabilities that can arise in the computations. In this method, $\overline{OP}$ is proportional to $\overline{OP_1} = (S_{ij}^d S_{ij}^d)^{3/2}$ and is inversely proportional to $\overline{OP_2} = (\bar{S}_{ij}\bar{S}_{ij})^{5/2} + (S_{ij}^d S_{ij}^d)^{5/4}$. The revised model is then obtained as

$$\nu_{\mathrm{SGS}}^{\mathrm{w}} = (C_w\Delta)^2\frac{\overline{OP_1}}{\overline{OP_2}} = (C_w\Delta)^2\frac{(S_{ij}^d S_{ij}^d)^{3/2}}{(\bar{S}_{ij}\bar{S}_{ij})^{5/2} + (S_{ij}^d S_{ij}^d)^{5/4}}, \tag{6}$$

where C_w is the model coefficient.

The WALE model takes into account the effects of the anti-symmetric part of the square of the velocity gradient tensor,[17] and the sub-grid stress near the wall is taken to be proportional to the third power of the distance from it.[18] These features were found to generally lead to improved predictions though the problem of producing too high levels of eddy viscosity remained, especially in the case of the massively separated flows that are of interest here.

In the regularized variational model (RVM) approach to LES, a sharp distinction is made between the wave numbers in the range $[0, k_{\max}/2]$ and those in the range $[k_{\max}/2, k_{\max}]$. Furthermore, the Smagorinsky eddy viscosity model is used for the high-pass filtered (HPF) field. With these adaptations, this model was found to produce improved results in some vortical flows.[19] The HPF velocity field $\tilde{\boldsymbol{u}}^{s^{(n)}}$ is computed from the difference between the LES velocity field $\bar{\boldsymbol{u}}$ and the low-pass filtered (LPF) field $\bar{\bar{\boldsymbol{u}}}^{(n)}$,

$$\tilde{\boldsymbol{u}}^{s^{(n)}} = \bar{\boldsymbol{u}} - \bar{\bar{\boldsymbol{u}}}^{(n)}. \tag{7}$$

Considering the filtering operators in three dimensional physical space, the LPF velocity field $\bar{\bar{\boldsymbol{u}}}$ is noted $\bar{\bar{u}}_i = \bar{G} * \bar{u}_i$ ($\bar{G}$ is the filter and $i = 1, 2, 3$) when the discrete filtering order n is equal to one. In the present work, the compact discrete filter ($\bar{G}$) is used due to its convenience, which only uses the nearest grid neighbors (stencil-3) to compute.[20,21] This filter is of second order and is tuned, so that its transfer function G goes to zero at the LES cutoff wavenumber ($kh = \pi$). For one dimensional space, it is applied to a function $f(x)$, namely, $\bar{u}$, and then the filtered $\bar{f}(x)$ is given as

$$\begin{aligned}\bar{f}(x) &= (\bar{G}^* f)(x)\\ &= f(x) + [f(x+h) - 2f(x) + f(x-h)]/4\\ &= f(x) + (\delta^2/4)f(x) = (I + \delta^2/4)f(x).\end{aligned}$$

With nonuniform grid spacing, the filtered $\bar{f}(x)$ is written as

$$\bar{f}(x) = [h_l(f(x+h_r) - f(x)) - h_r(f(x) - f(x-h_l))]/(2(h_l + h_r)) + f(x),$$

where h is the grid spacing and $\delta^2/4$ is an operator used for shorter notation. h_l and h_r are the spacing on the left and right sides of x, respectively.

Expanding three dimensions field, $\bar{\bar{\boldsymbol{u}}}^{(n)}$ is obtained by operating one direction at a time of stencil three explicit discrete filter (tensor products, $\bar{G} = \overline{G_x} * \overline{G_y} * \overline{G_z}$),

$$\bar{\bar{\boldsymbol{u}}}^{(n)} = \left\{\left[I - (-\delta_x^2/4)^n\right]\left[I - (-\delta_y^2/4)^n\right]\left[I - (-\delta_z^2/4)^n\right]\right\}\bar{\boldsymbol{u}}, \tag{8}$$

where I is the identity operator, $\delta_x^2 f_{i,j,k} = f_{i+1,j,k} - 2f_{i,j,k} + f_{i-1,j,k}$ (on a uniform grid), n is the filtering order of the discrete filter. $n = 1$ represents second-order filter operator; $n = 2$ represents fourth-order filter operator. In the present work, n was taken as 2, and then $\tilde{\boldsymbol{u}}^{s^{(n)}}$ was simplified as $\tilde{\boldsymbol{u}}^s$.

By substituting Eq. (8) into Eq. (7), $\tilde{\boldsymbol{u}}^s$ can be solved. Then, by using $\tilde{\boldsymbol{u}}^s$ to replace the velocity field $\bar{\boldsymbol{u}}$ in Eq. (4), τ_{ij} can be now be rewritten as

$$\tilde{\tau}_{ij}^s = 2\nu_{\mathrm{SGS}}^s\tilde{S}_{ij}^s = 2C\Delta^2|\tilde{S}_{ij}^s|\tilde{S}_{ij}^s, \tag{9}$$

where ν_{SGS}^s is the eddy viscosity of SGS. $\tilde{S}_{ij}^s = \frac{1}{2}(\frac{\partial \tilde{u}_i^s}{\partial x_j} + \frac{\partial \tilde{u}_j^s}{\partial x_i})$ and $\tilde{\tau}_{ij}^s$ are the strain-ratio tensor and the sub-grid stress tensor in the HPF field, respectively.

This model, while possessing the necessary dependencies that render it suitable for use in multiscale flows, nevertheless, still produces too high values of SGS dissipation close to solid walls. This is because the LES flow is still unsteady and anisotropic in the near-wall region, and $\tilde{S}_{ij}^s$ is not equal to zero, which results in significant spatial nonuniformity.[8,10]

Considering the advantages of small scales locally of RVM and the natural near-wall damping behavior of the WALE model, it seemed logical to introduce the HPF field in the RVM into the traditional WALE model in order to benefit from the advantages of both

Published under an exclusive license by AIP Publishing

approaches. This is done here by using $\tilde{\boldsymbol{u}}^s$ (the HPF field) to replace $\bar{\boldsymbol{u}}$ (the filtered field) in $\bar{S}_{ij}$ in Eq. (4), and S^d_{ij} in Eq. (5). Thereafter, according to the algorithm of Eq. (6), ν^{sw}_{SGS} is rewritten as

$$\nu^{sw}_{\mathrm{SGS}} = (C_w\Delta)^2 \frac{(\tilde{S}^{sd}_{ij}\tilde{S}^{sd}_{ij})^{3/2}}{(\tilde{S}^{s}_{ij}\tilde{S}^{s}_{ij})^{5/2} + (\tilde{S}^{sd}_{ij}\tilde{S}^{sd}_{ij})^{5/4}}. \tag{10}$$

Substituting Eq. (10) into Eq. (4), the SGS stress in the HPF field is obtained as

$$\tilde{\tau}^{sw}_{ij} = 2\nu^{sw}_{\mathrm{SGS}}\tilde{S}^{s}_{ij} = (C_w\Delta)^2 \frac{(\tilde{S}^{sd}_{ij}\tilde{S}^{sd}_{ij})^{3/2}}{(\tilde{S}^{s}_{ij}\tilde{S}^{s}_{ij})^{5/2} + (\tilde{S}^{sd}_{ij}\tilde{S}^{sd}_{ij})^{5/4}}\tilde{S}^{s}_{ij}, \tag{11}$$

where $\tilde{S}^{s}_{ij}$ and $\tilde{S}^{sd}_{ij}$ are the strain-rate tensor and the deviatoric part of the tensor $\left(\tilde{S}^{sd}_{ij} = \frac{1}{2}\left(\frac{\partial\tilde{u}^s_i}{\partial x_k}\frac{\partial\tilde{u}^s_k}{\partial x_j} + \frac{\partial\tilde{u}^s_j}{\partial x_k}\frac{\partial\tilde{u}^s_k}{\partial x_i}\right)\right)$, respectively. C_w is a constant that is assigned the value of 0.5 suggested by Nicoud and Ducros.[4] As will be shown below, computations in which this constant was varied in the range 0.35–0.50 yielded no discernable differences.

In the extended WALE model, the sub-grid stress ($\tilde{\tau}^{sw}_{ij}$) in Eq. (11) is used to close the governing equations. The use of this method ensures a natural near-wall damping behavior. It also guarantees that the model is active for when there are small scales (high wave numbers) in the LES field, so it has a good spectral behavior in turbulence at the high Reynolds number.

III. LES OF FLOW AROUND A CYLINDER

The turbulent flow around a circular cylinder at high Reynolds number presents an exacting test for LES models due to the occurrence of massively separated regions in which the organized mean-flow periodicity due to vortex shedding interacts with the small-scale turbulent motions. This flow has been the subject of numerous computational and experimental studies (Lourenco and Shih;[22] Sircar *et al.*,[14] Parnaudeau *et al.*,[23] Ong and Wallace,[24] Lim and Lee,[25] Norberg[26]). In this work, we assess the extended WALE model against data at two different Reynolds numbers, viz., $Re = 3.9 \times 10^3$ and $Re = 4.0 \times 10^4$.

A. Computational details

The computational domain of the flow around a cylinder (Fig. 1) extends to a distance of 29D in the streamwise direction with the inlet boundary being located at distance 8.5D upstream of the leading edge. The outflow boundary was located at 19.5D downstream of the trailing edge. In the y direction, the computational domain extended to a distance of 7.5D from the cylinder's center and πD along the span of cylinder.

The computations were performed on a structured hexahedral mesh with an O-topology being used around the cylinder to exactly match the surface. The computational mesh consisted of 607 450 active cells (Fig. 1). In the near wall region, the first layer of grid is $y^+ = 2.5$ to improve as much as possible the accuracy of the calculations while remaining within reasonable limits in terms of computational resources. The grid expansion ratio was limited to 1.05. The grid nodes in the circumferential direction and along the span were set to 400 and 11, respectively. Details of the computational domain are given in Table I.

The boundary conditions used for the computations were as follows: at inlet, a uniform velocity profile was prescribed corresponding

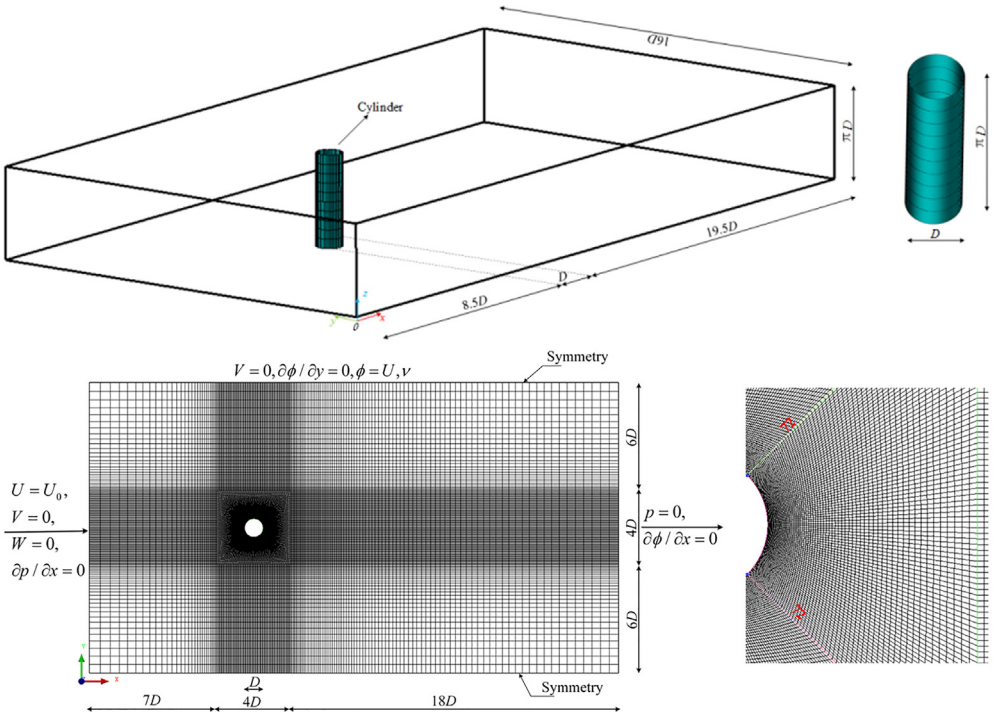

FIG. 1. Schematic of the computational domain and grid distribution for $Re = 3.9 \times 10^3$.

Published under an exclusive license by AIP Publishing

TABLE I. Details of the computational domain and grid at $Re = 3.9 \times 10^3$.

				Mesh number	
	L_x	L_y	L_z	$N\,(10^6)$	N_z
Present work	$29D$	$16D$		0.61	11
Parnaudeau *et al.*[23]	$20D$	$20D$		44.28	48
Dmitry *et al.*[27]	$50D$	$50D$	πD	5.76	64
Sircar *et al.*[14]	$25D$	$20D$		4.81	40
Wornom *et al.*[28]	$35D$	$40D$		1.80	100

to the value of Reynolds number. At outlet, the pressure was set to zero. At the top, bottom, and side boundaries of three dimensional domains, plane-of-symmetry boundary conditions were applied (see Fig. 1). The no-slip condition was applied at the walls. The computational time step is set to be 0.05 s for $Re = 3.9 \times 10^3$ and 0.005 s for $Re = 4 \times 10^4$ to ensure the Courant–Friedrichs–Lewy number is less than 1. Iterations were performed at each time step with the convergence criterion taken to be when the absolute sum of all residuals fell to a value below 10^{-6}.

B. Results and discussion

In order to validate computational accuracy of the extended WALE model for the near wall velocity, simulations of flow around a cylinder at $Re = 3.9 \times 10^3$ were compared to the results from using the standard WALE model and the Dyn K-eqn model (Sircar *et al.*[14]). Figure 2 shows the circumferential distribution of the non-dimensional friction velocity $\bar{u}_\tau/U (= \sqrt{\tau_w/\rho}/U$, where τ_w is the shear stress and U is the velocity of the incident flow) along the cylinder surface. Plotted there are the results obtained with both the original and the extended WALE models, the latter obtained with three different values for the coefficient C_w (viz. 0.35, 0.45, and 0.50) to explore the sensitivity of this model's performance to the value assigned to this coefficient. The differences between the different results of the extended model are hardly discernable. The profile of $\bar{u}_\tau/U$ obtained using the extended WALE model compares very well with the Dyn K-eqn model, with both obtaining values higher than those obtained with the original WALE model, especially at the peak of $\theta = 45°$. At this point, $\bar{u}_\tau/U$ reaches a maximum, due to flow attachment from the surface and transition from a laminar boundary layer to a turbulent one. The original WALE model obtains a significantly lower value there. With the increase in the θ value, $\bar{u}_\tau/U$ decreases to reach a minimum value near $\theta = 90°$ due to the reduction in skin friction, and then it approximately approaches a roughly constant at the rear of the cylinder that is seen to be in close agreement with the Dyn K-eqn model results.

In the study of flow development in the rear of the cylinder, the extent of the recirculation zone is considered another one of the most important flow features for the flow past cylinder because it is a region of large shear stresses, and hence, most of the turbulence production due to the interaction of the shear with the mean flow occurs here. To evaluate the ability of the extended WALE model to capture this feature of the flow, predictions of the time-averaged recirculation bubble length L_r are presented. This parameter, presented in non-dimensional form as L_r/D, is defined as the distance between the base of the cylinder to the point where the sign of the centerline mean streamwise velocity changes from negative to positive. Figure 3 compares the predicted and measured mean streamwise velocity along the centerline. In this and subsequent figures, $x = 0$ corresponds to the center of the cylinder. The value of L_r/D predicted by the extended WALE model was 1.20, which is in good agreement with the value of 1.19 suggested by the measurements of Lourenco and Shih.[22] In contrast, the values of L_r/D predicted by the WALE and the K-eqn models were 0.9 and 1.67, respectively. In this regard, it should be noted that the particle image velocimetry (PIV) data provided by Parnaudeau *et al.*[23] revealed a more extended recirculation zone length $L_r/D = 1.36$–1.51. Nevertheless, it can be seen in Fig. 3 that with the increase in x/D, the change of $\langle\bar{u}\rangle/U$ predicted by the extended WALE model provides the closest agreement with the experiments.

The velocity distribution in the wake of the cylinder was investigated to gain further insight into the model's performance in the

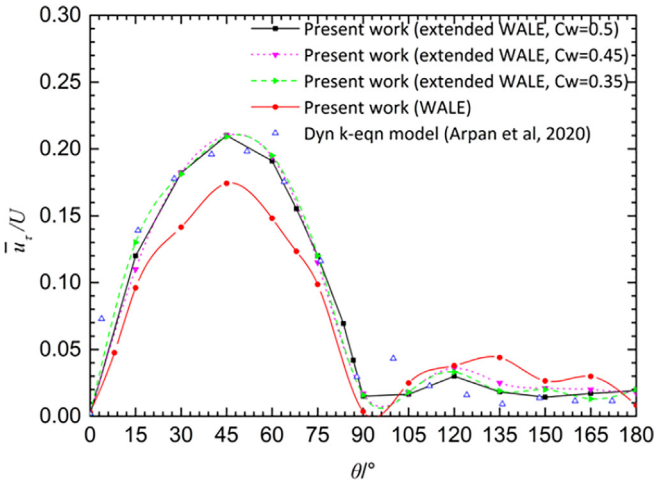

FIG. 2. Distribution of friction velocity along the cylinder surface.

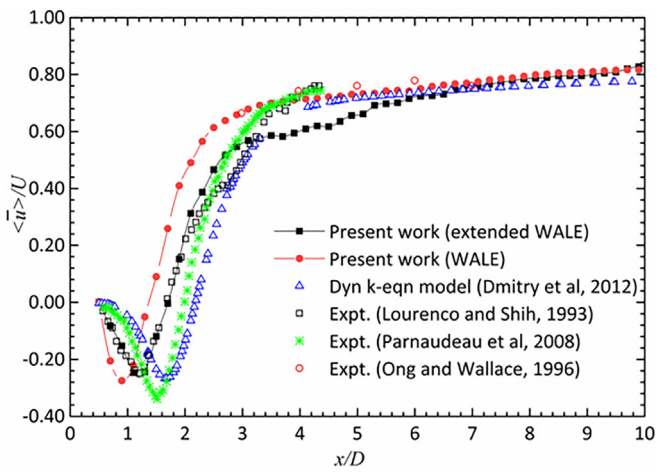

FIG. 3. Mean stream-wise velocity along the wake centerline.

Published under an exclusive license by AIP Publishing

separated flow zone. Figure 4 shows the centerline values of the mean and fluctuating velocity components in the streamwise and transverse directions. As can be seen in Fig. 4(a), the present predictions of $\langle\bar{u}\rangle/U$ by the extended WALE are very consistent with the experimental results of Lourenco and Shih.[22] Some differences are observed with respect to the measurements of Parnaudeau *et al.*[23] and Ong and Wallace.[24] Such differences are to be expected considering the different experimental conditions and measurement techniques employed in these studies. Lourenco and Shih[22] used particle image velocimetry to measure the recirculation bubble downstream of a cylinder in a towing tank facility ($Re = 3.9 \times 10^3$). The results were obtained from 93 instantaneous velocity field images spanning 29 vortex shedding cycles. In contrast, the experiments of Parnaudeau *et al.*[23] and Ong and Wallace[24] were conducted in a wind tunnel using hot-wire anemometry. Such differences in experimental techniques and set-ups can be expected to yield the degree of differences observed in the experimental data. Figure 4(b) presents the profile of mean transverse velocity $\langle\bar{v}\rangle/U$ at the same streamwise positions. Due to the occurrence of alternate vortex shedding, the profile of $\langle\bar{v}\rangle/U$ is antisymmetric along centerline of cylinder. The present results are in generally good agreement with the direct numerical simulation (DNS) results of Tremblay *et al.*[29] at $x/D = 1.06$. In this region, $\langle\bar{v}\rangle/U$ is somewhat overestimated in the WALE model because the prediction of the recirculation zone length was underestimated, while it is somewhat underestimated in the Dyn K-eqn results and experimental results of Parnaudeau *et al.*[23] due to over prediction of recirculation zone length. At $x/D = 2.02$ and 4.00, good agreement was observed between the extended WALE and the Dyn K-eqn model results and the experimental data of Lourenco and Shih,[22] Parnaudeau *et al.*,[23] and Ong and Wallace.[24] It can also be seen from the close-up plots in Figs. 4(a) and 4(b) that the predicted $\langle\bar{u}\rangle/U$ by the three models, especially near the centerline of the wake of cylinder at $x/D = 4.00$, marginally underestimate the experimental results.[24] The overall trend change is consistent. Moreover, the predicted $\langle\bar{v}\rangle/U$ by the WALE model is also larger than experimental results, especially as y/D is in the range of 0 to 1 at $x/D = 4.00$. This indicates that the dissipation of the WALE model along the streamwise is larger than in the transverse direction.

Comparisons of streamwise and transverse velocity fluctuations for the very near wake ($1 \le x/D \le 4$) are shown in Figs. 4(c) and 4(d). Due to the transitional state of the shear layers, $\langle\bar{u}'\bar{u}'\rangle/U^2$ profile presents two prominent peaks: at $x/D = 1.06$ and 2.02. The extended WALE predictions agree fairly closely with the experimental data at those different downstream locations, but the magnitudes of the peaks were larger for the WALE model results and smaller for the Dyn K-eqn model results. At $x/D = 4.00$, all three models yield results that closely match the measurements of Ong and Wallace[24] as y/D is far from the

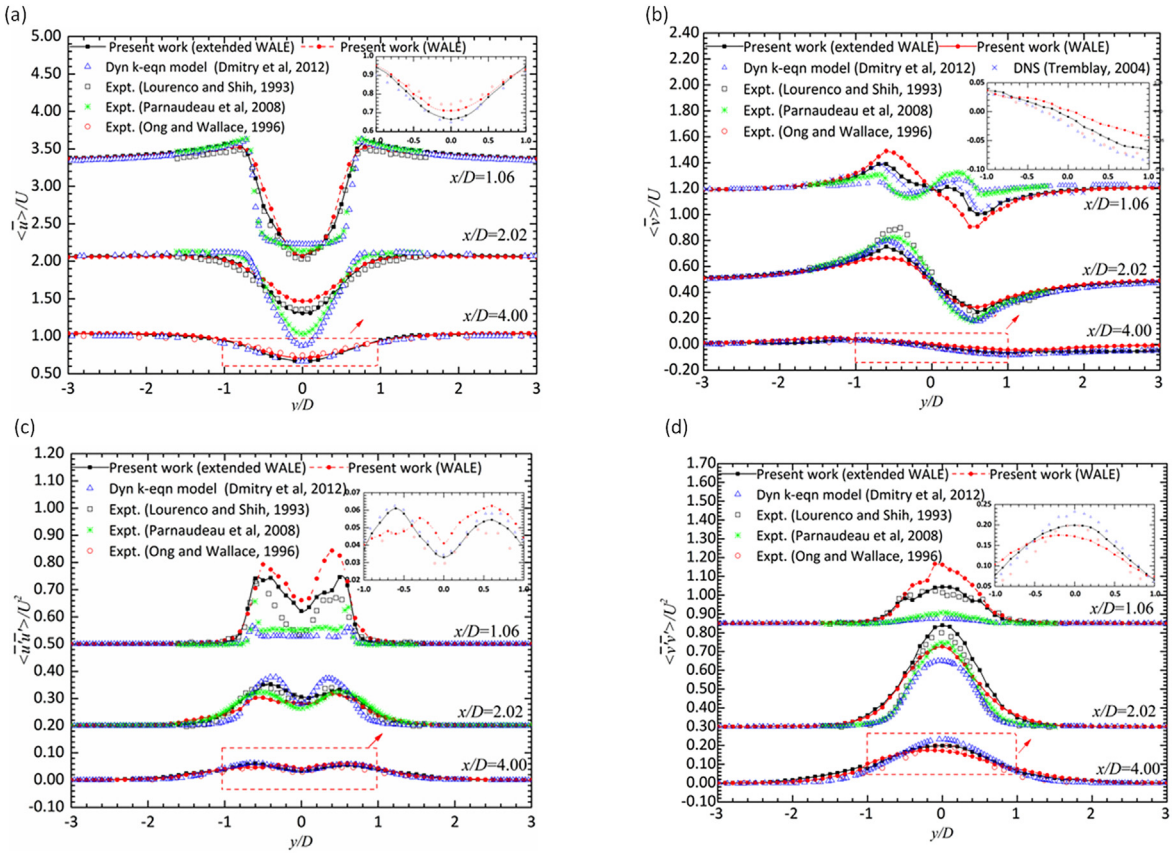

FIG. 4. Fluctuating velocity variation at different locations in the wake of the cylinder ($Re = 3.9 \times 10^3$). (a) Mean stream-wise velocity. (b) Mean transverse velocity. (c) Mean stream-wise Reynolds stress. (d) Mean transverse Reynolds stress.

Published under an exclusive license by AIP Publishing

centerline of the cylinder, while the predicted $\langle \bar{v}'\bar{v}' \rangle / U^2$ by the extended WALE model is in better agreement with the experiment[24] near wake centerline. Figure 4(d) presents the profiles of the transverse velocity fluctuations $\langle \bar{v}'\bar{v}' \rangle / U^2$. It is seen there that a single peak appears along the centerline of wake ($y/D = 0$). It can also be seen that the extended WALE results are in good agreement with the experimental data in the very near wake. However, the WALE model results show that the peak value was overestimated at $x/D = 1.06$, which implies that the laminar-turbulent transition of the separated shear layers occurs nearer to the cylinder, which leads to a shorter L_r/D. In contrast, the Dyn K-eqn model results underestimated magnitude of $\langle \bar{v}'\bar{v}' \rangle / U^2$, such that a longer L_r/D is obtained. Further downstream, the differences among three models became smaller.

Attention is now turned to the higher Reynolds-number case. Figure 5 shows comparisons of the velocity variation along the stream-wise and transverse directions in the cylinder wake at $Re = 4 \times 10^4$. It can be seen from Fig. 5(a) that the predicted $\langle \bar{u} \rangle / U$ profiles for both the extended and the original WALE models are similar with L_r/D

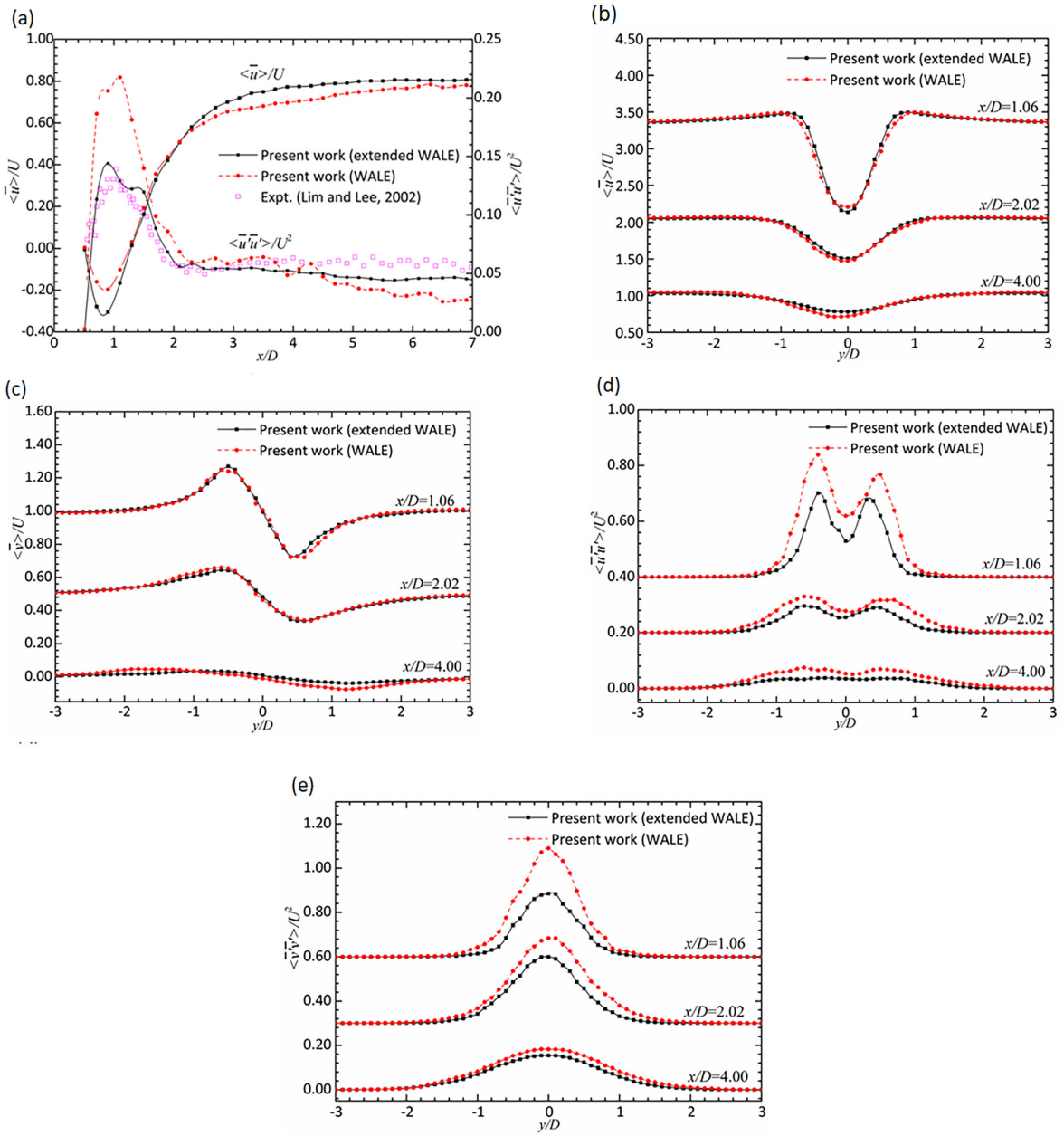

FIG. 5. Velocity variation at different locations in the separated wake ($Re = 4 \times 10^4$). (a) Mean and fluctuating velocity along stream-wise direction. (b) Mean stream-wise velocity. (c) Transverse velocity. (d) Stream-wise velocity fluctuations. (e) Transverse velocity fluctuations.

Published under an exclusive license by AIP Publishing

predicted as 0.82 and 0.88, respectively. However, the extended WALE result is in better agreement with the data of Wornom *et al.*[28] and Salvatici and Salvetti[30] ($L_r/D = 0.8$ and 0.77–0.86). Moreover, the minimum of $\langle\bar{u}\rangle/U$ was slight larger. For $\langle\bar{u}'\bar{u}'\rangle/U^2$, it is clear that the profile obtained using the extended WALE model compares very well with the experimental data of Lim and Lee.[25] The standard WALE model, in contrast, does not yield the correct profile of streamwise velocity fluctuations at $0.25 \leq x/D \leq 2$. Figures 5(b) and 5(c) compare the velocity profiles predicted by the present models. The agreement between the predicted and measured mean velocity is very good at the different streamwise directions. At $Re = 4 \times 10^4$, the distribution shapes of mean velocity were similar to the case of $Re = 3.9 \times 10^3$. However, the predicted profiles of $\langle\bar{u}'\bar{u}'\rangle/U^2$ and $\langle\bar{v}'\bar{v}'\rangle/U^2$ were greatly different. It can be seen from Figs. 5(d) and 5(e) that the predicted fluctuating velocity by the standard WALE model is larger than that of extended WALE model near the centerline of cylinder at $x/D = 1.06$. This indicates that the predicted Reynolds stresses were overestimated due to the underestimation of L_r.

Figure 6 presents comparisons of the instantaneous iso-surface vorticity formation as obtained by the extended and the original

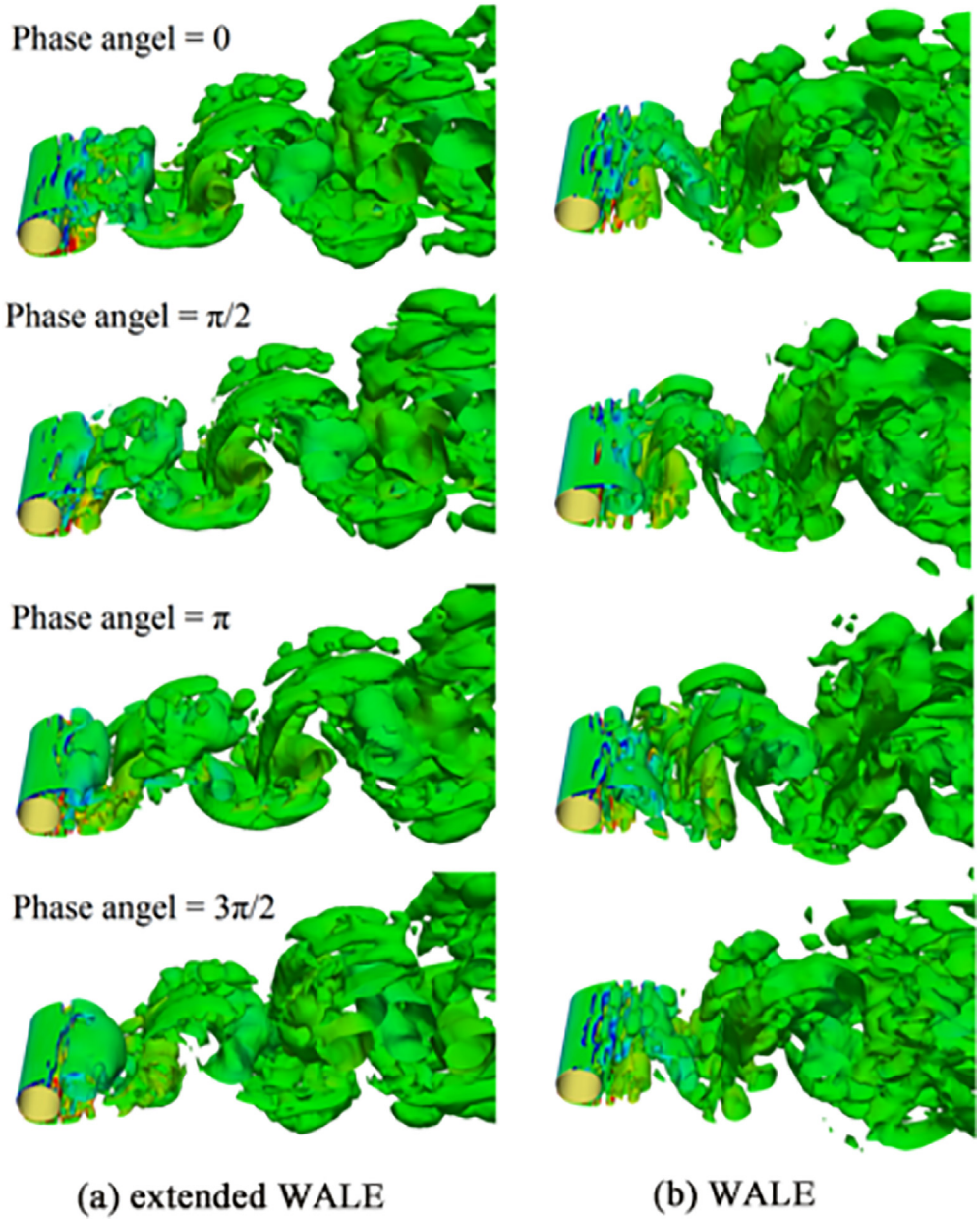

FIG. 6. Iso-surface of z-component of vorticity for flow over a circular cylinder at $Re = 3.9 \times 10^3$. (a) extended WALE. (b) WALE.

Published under an exclusive license by AIP Publishing

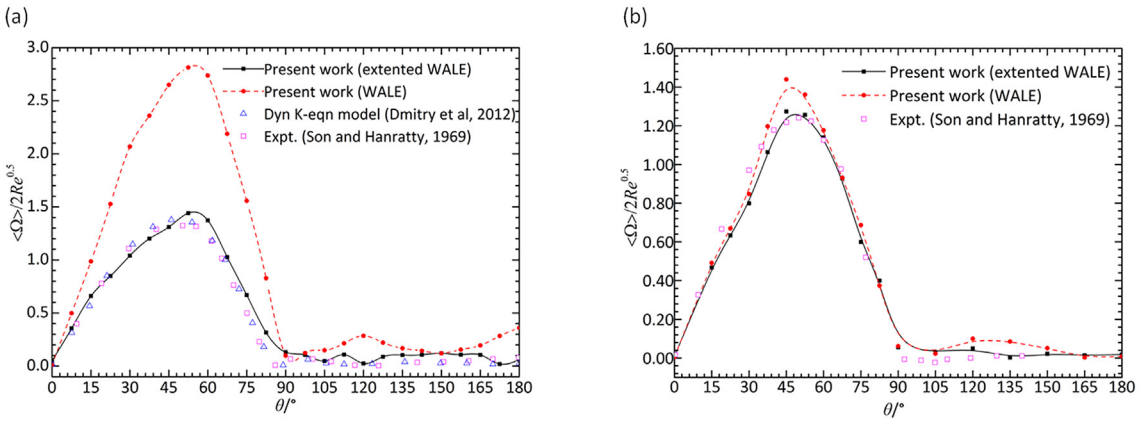

FIG. 7. Distributions of normalized mean vorticity on the cylinder surface. (a) $Re = 3.9 \times 10^3$. (b) $Re = 4 \times 10^4$.

WALE models within a vortex shedding cycle. There are clearly some differences in the predicted distribution of vorticity in the near wake of the cylinder. It can be observed that the fluctuation and breakup of vorticity by the standard WALE model are significantly more pronounced than that obtained by the extended model. Moreover, the distribution of the vorticity near rear cylinder surface is not very smooth.

Figure 7 shows the comparisons of the mean vorticity distributions on the surface of cylinder at $Re = 3.9 \times 10^3$ and $Re = 4 \times 10^4$. It can be seen in Fig. 7(a) that predicted vorticity distributions by the extended WALE and Dyn K-eqn models are very consistent with the experimental data (Son and Hanratty[31]) at both Reynolds numbers. In contrast, the WALE model results appear to overestimate the measurements for $\theta < 90°$ at $Re = 3.9 \times 10^3$. For the flow at Reynolds number of $Re = 4 \times 10^4$, the predicted vorticity by the extended WALE matched very well with the experimental results (Son and Hanratty[31]). The predicted vorticity obtained by the WALE model is also consistent with the experimental data, but the peak value was somewhat larger at $\theta \approx 45°$. This indicates that predicted vorticity was overestimated. Taken together, these features indicate that the dissipation of the original model is much greater than that of the extended version.

Comparisons of the power spectra for $Re = 3.9 \times 10^3$ and 4×10^4 are presented in Fig. 8. These results were extracted from 50 vortex shedding cycles at the downstream location on the centerline of the wake ($x/D = 3$). The fast Fourier transform (FFT) technique was used to obtain the spectra. The frequency (f) was non-dimensionalized by the Strouhal shedding frequency (f_{vs}). It can be seen in Fig. 8(a) that the predicted power spectra obtained by the extended WALE and the Dyn K-eqn models yielded a good overall agreement with the experimental spectrum (Lourenco and Shih,[22] Parnaudeau *et al.*[23]), reproducing well the two peaks of power spectra well at $f/f_{vs} = 1$ and 3. In contrast, the spectra by the standard WALE model do not match well with experimental results in the range $0.55 < f/f_{vs} < 3.0$. It is also noticeable that the dissipation ranges obtained by the three models were very similar, so the spectrum started to decay rapidly before the grid frequency cutoff. For $Re = 4 \times 10^4$, due to lack of data, Fig. 8(b) presents comparisons of only the present predictions. Overall, the differences in the power spectrum results between the extended and the original formulations are small.

The predicted and measured distributions of the mean surface pressure are displayed in Fig. 9. It can clearly be seen that the extended

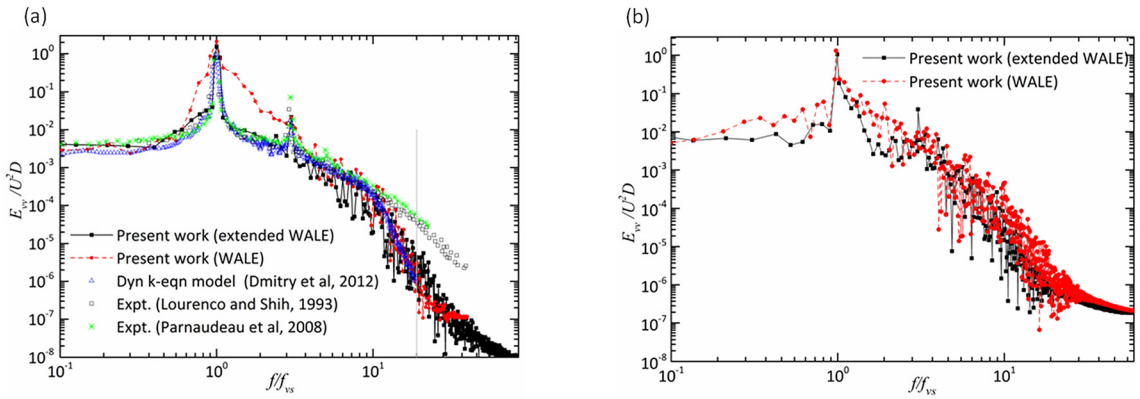

FIG. 8. Power spectra of the transverse velocity in the wake of the cylinder ($x/D = 3$). (a) $Re = 3.9 \times 10^3$. (b) $Re = 4 \times 10^4$.

Published under an exclusive license by AIP Publishing

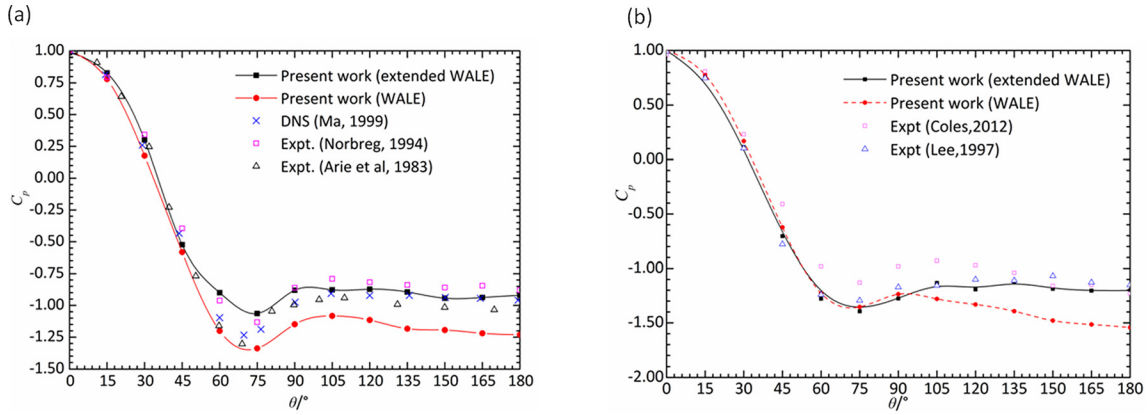

FIG. 9. Distribution of mean pressure coeffcient on the cylinder surface. (a) $Re = 3.9 \times 10^3$. (b) $Re = 4 \times 10^4$.

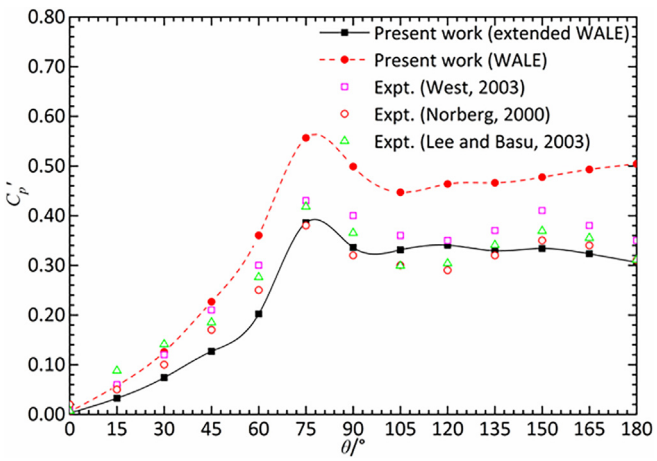

FIG. 10. Distribution of fluctuating pressure coeffcient on the cylinder surface ($Re = 4 \times 10^4$).

WALE model predictions for this parameter match very closely with the experimental data of Norberg,[32] Arie *et al.*,[33] Cantwell and Coles,[34] and Lee and Basu[35] for both values of Reynolds numbers. In contrast, the standard WALE model consistently underestimates this parameter, especially over the base of the cylinder downstream of the point of flow separation. Figure 10 presents comparisons between the predicted and measured surface pressure fluctuations. Here again, it is evident that the extended model produces far closer agreement with the measurements of West and Apelt,[36] Norberg,[37] and Lee and Basu[35] than that obtained with the original model.

Figure 11 shows the time history of the lift and drag coefficients as predicted by the two WALE models. The time axis is non-dimensionalized as $t^* = Ut/D$. It is clear that both the lift and the drag coefficients computed by the WALE model show greater departures from the mean values compared with the extended model's results. Quantitative comparisons are given in Table II. It is clear that predicted bulk coefficients ($\langle C_d \rangle$, C_l', St) obtained with the extended WALE model provide a close match to the experimental values (Norberg,[26] Prsic *et al.*[38]) at both Reynolds numbers. In contrast, the

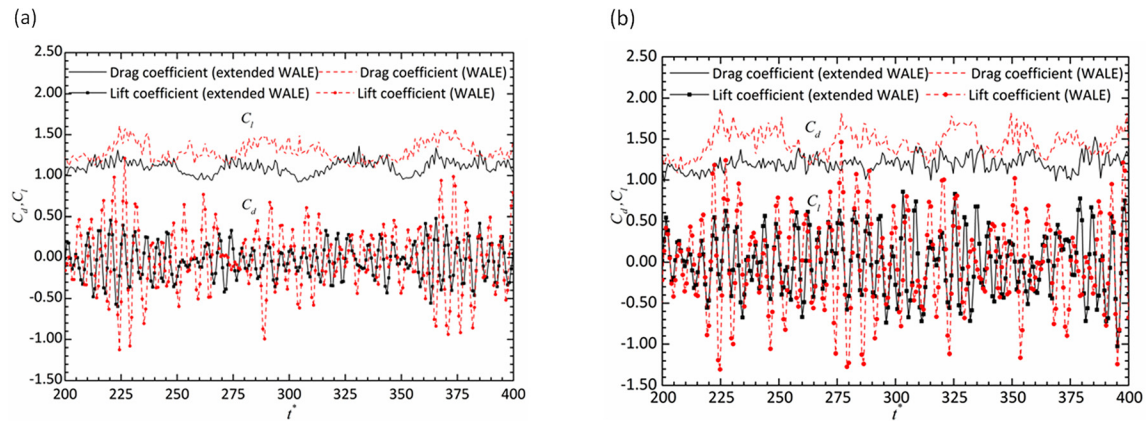

FIG. 11. Time histories of the lift and drag coeffcients. (a) $Re = 3.9 \times 10^3$. (b) $Re = 4 \times 10^4$.

Published under an exclusive license by AIP Publishing

TABLE II. Computed and measured lift and drag coeffcients and Strouhal number.

	$Re = 3.9 \times 10^3$			$Re = 4 \times 10^4$			
Parameters	$\langle C_d \rangle$	C_l'	St	$\langle C_d \rangle$	C_d'	C_l'	St
Present work (extended WALE)	1.07	0.23	0.21	1.15	0.10	0.41	0.21
Present work (WALE)	1.21	0.40	0.21	1.42	0.17	0.55	0.18
Expt. (Norberg[26])	0.99 ± 0.05	⋯	0.21–0.22	⋯	⋯	⋯	⋯
Smag. (Prsic *et al.*[38])	1.10	0.20	0.22	⋯	⋯	⋯	⋯
Measurements	⋯	⋯	⋯	0.90–1.15[a]	0.137[b]	0.20–0.50[c]	0.196[d]
Expt. (Bouak and Lemay[39])	⋯	⋯	⋯	1.20	0.11	0.43	0.20

[a]DuarteRibeiro,[40] $\mathrm{Re} = 4.0 \times 10^4 - 3.5 \times 10^5$.
[b]West and Apelt,[36] $\mathrm{Re} = 4.4 \times 10^4$, 6.6×10^4.
[c]Humphreys,[41] $\mathrm{Re} = 3.0 \times 10^4 - 5.7 \times 10^5$.
[d]Ma *et al.*,[42] $\mathrm{Re} = 5.0 \times 10^4 - 4.5 \times 10^5$.

predicted mean drag coefficients by the standard WALE model are higher than the consensus of the experimental data while the fluctuating lift and drag coefficients (C_l', C_d') are overestimated by as much as a factor of 2.

IV. CONCLUSIONS

The paper describes the extension of the well-established WALE model for the treatment of the near-wall region in large-eddy simulations to more accurately predict the multi-scale flows over complex structure. The extended model involves combining the wall-adapting local eddy viscosity model with the regularized variational multiscale model in order to decrease the excessive dissipation associated with the former, and to better capture the correct asymptotic near-wall behavior. The performance of this model, which was implemented in the OpenFOAM toolbox, was assessed for the difficult case of turbulent flows around a circular cylinder at two values of Reynolds number, namely, $Re = 3.9 \times 10^3$ and $Re = 4 \times 10^4$. Predicted instantaneous flow features and bulk flow parameters, such as mean and fluctuating lift and drag coefficients and Strouhal number, were compared with benchmark experimental data and with results from the original WALE and Dyn K-eqn models. The results show that the extended model yields significantly better predictions of the complex features of these flows than the original formulation. While the improvements have been amply demonstrated for this challenging class of flows, it remains to be seen whether they will be obtained in all classes of flow that may be of general interest.

ACKNOWLEDGMENTS

We gratefully acknowledge the support provided by the National Natural Science Foundation of China (Grant No. 11472087 and No. 11002038).

AUTHOR DECLARATIONS

Conflict of Interest

The authors have no conflicts to disclose.

DATA AVAILABILITY

The data that support the findings of this study are available from the corresponding author upon reasonable request.

APPENDIX: OPENFOAM IMPLEMENTATION

The extended WALE model was implemented in OpenFOAM. The program body of the extended WALE model was performed in the source file (*.C file), and various libraries and basic classes called by the source file were declared in the header file (*.H file). In Make folder, we specified the storage location of the compiled source file and the declaration location of the header file. Then, dynamic procedure (*.so file) was generated by "wmake" command to use for dynamic invocation. In the process of using the implemented extended WALE model to simulate various turbulent flows, these partial differential equations to be solved can be represented by the class of OpenFOAM. Taking the standard momentum equation as an example, the description is as follows:

$$\frac{\partial \rho \boldsymbol{u}}{\partial t} + \nabla \cdot (\rho \boldsymbol{u}\boldsymbol{u}) - \nabla(\mu \nabla \boldsymbol{u}) = -\nabla p.$$

This equation discretized based on the finite volume method can be presented as follows:

```
Solve
(fvm::ddt(rho, u)
+ fvm::div(phi, u)
- fvm::laplacian(mu, u)
==
- fvc::grad(p)
);
```

In the present paper, time discretization adopts implicit second-order accurate scheme, which was a multi-step backward lattice scheme. The spatial discrete scheme was also second-order scheme. The linear-upwind stabilized transport (LUST) scheme[43] was applied to discretize the convection term to avoid short wavelength oscillations (Cao and Tamura,[44] Mukha *et al.*[45]). The LUST scheme is a hybrid scheme by 75% linear scheme and 25%

Published under an exclusive license by AIP Publishing

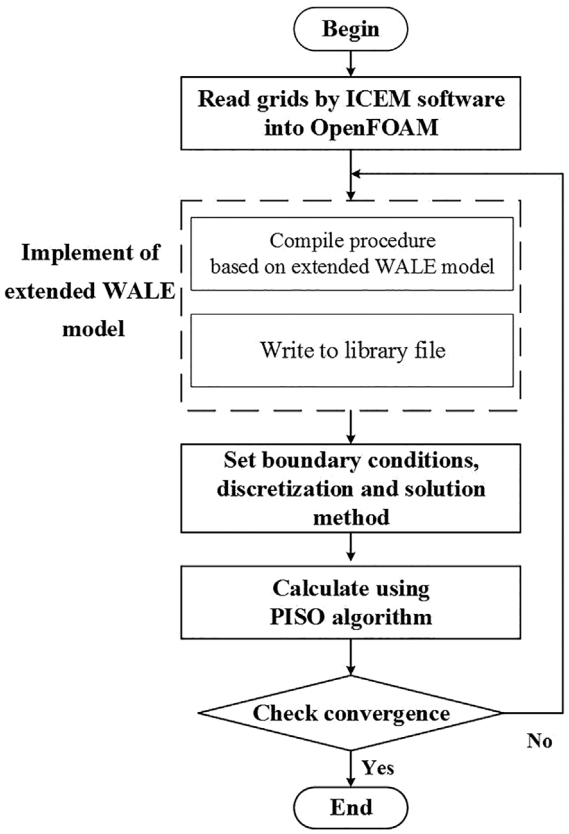

FIG. 12. Basic chart of numerical calculation.

linearUpwind scheme. For the Laplacian term and gradient terms, they were discretized by Gauss linear corrected scheme and Gauss linear scheme, respectively. Moreover, pressure-implicit with splitting of operators (PISO) algorithm was applied to solve iteratively. The chart of calculation is shown in Fig. 12.

REFERENCES

[1]H. Kobayashi, "Large eddy simulation of magnetohydrodynamic turbulent channel flows with local subgrid-scale model based on coherent structures," Phys. Fluids **18**, 045107 (2006).

[2]K. S. Chang, B. S. Yoon, and J. S. Lee, "Large eddy simulation of magnetohydrodynamic turbulent channel flows with local subgrid-scale model based on coherent structures," Eng. Appl. Comput. Fluid Mech. **16**, 49 (2011).

[3]J. Smagorinsky, "General circulation experiments with the primitive equations: I. The basic experiment," Mon. Weather Rev. **91**, 99 (1963).

[4]F. Nicoud and F. Ducros, "Subgrid-scale stress modelling based on the square of the velocity gradient tensor," Flow Turbul. Combust. **62**, 183 (1999).

[5]S. M. Modirkhazeni, V. G. Bhigamudre, and J. P. Trelles, "Evaluation of a non-linear variational multiscale method for fluid transport problems," Comput. Fluids **209**, 104531 (2020).

[6]Z. Liu, Y. Wu, and B. Li, "An assessment on the performance of sub-grid scale models of large eddy simulation in modeling bubbly flows," Powder Technol. **374**, 470 (2020).

[7]T. Hughes, L. Mazzei, A. A. Oberai, and A. A. Wray, "The multiscale formulation of large eddy simulation: Decay of homogeneous isotropic turbulence," Phys. Fluids **13**, 505 (2001).

[8]G. Winckelmans and H. Jeanmart, "Direct and large-eddy simulation IV," in *ERCOFTAC Series*, Vol. 8, edited by B. J. Geurts, R. Friedrich, and O. Métais (Kluwer, Dordrecht, 2001), pp. 55–66.

[9]S. C. Kassinos, C. A. Langer, G. Iaccarino, and P. Moin, "Complex effects in large eddy simulations," in *Lecture Notes in Computational Science and Engineering* (Springer Science & Business Media, 2007), Vol. 56.

[10]H. Jeanmart and G. Winckelmans, "Investigation of eddy-viscosity models modified using discrete filters: A simplified 'regularized variational multiscale model' and an 'enhanced field model'," Phys. Fluids **19**, 055110 (2007).

[11]M. Montecchia, G. Brethouwer, A. V. Johansson, and S. Wallin, "Taking large-eddy simulation of wall-bounded flows to higher Reynolds numbers by use of anisotropy-resolving subgrid models," Phys. Rev. Fluids **2**, 034601 (2017).

[12]J. D. Tellez-Alvarez, K. Koshelev, S. Strijhak, and J. M. Redondo, "Simulation of turbulence mixing in the atmosphere boundary layer and analysis of fractal dimension," Phys. Scr. **94**, 064004 (2019).

[13]A. K. Shukla and A. Dewan, "OpenFOAM based LES of slot jet impingement heat transfer at low nozzle to plate spacing using four SGS models," Heat Mass Transfer **55**, 911 (2019).

[14]A. Sircar, M. Kimber, S. Rokkam, and G. Botha, "Turbulent flow and heat flux analysis from validated large eddy simulations of flow past a heated cylinder in the near wake region," Phys. Fluids **32**, 125119 (2020).

[15]A. P. Zahiri and E. Roohi, "Anisotropic minimum-dissipation (AMD) subgrid-scale model implemented in OpenFOAM: Verification and assessment in single-phase and multi-phase flows," Comput. Fluids **180**, 190 (2019).

[16]J. Gonzalez-Trejo, C. A. Real-Ramirez, I. Carvajal-Mariscal, F. Sanchez-Silva, F. Cervantes-De-La-Torre, R. Miranda-Tello, and R. Gabbasov, "Hydrodynamic analysis of the flow inside the submerged entry nozzle," Math. Probl. Eng. **2020**, 6267472.

[17]H. Zhu, W. Liu, and T. Zhou, "Direct numerical simulation of the wake adjustment and hydrodynamic characteristics of a circular cylinder symmetrically attached with fin-shaped strips," Ocean Eng. **195**, 106756 (2020).

[18]A. Luo, "On flow switching bifurcations in discontinuous dynamical systems," Commun. Nonlinear Sci. **12**, 100 (2007).

[19]R. Cocle, L. Bricteux, and G. Winckelmans, "Scale dependence and asymptotic very high Reynolds number spectral behavior of multiscale subgrid models," Phys. Fluids **21**, 085101 (2009).

[20]T. Brandt, "Usability of explicit filtering in large eddy simulation with a low-order numerical scheme and different subgrid-scale models," Int. J. Numer. Methods Fluids **57**, 905 (2008).

[21]O. Vasilyev, T. Lund, and P. Moin, "A general class of commutative filters for LES in complex geometries," J. Comput. Phys. **146**, 82 (1998).

[22]L. M. Lourenco and C. Shih, Characteristics of the plane turbulent near wake of a cylinder. A particle image velocimetry study, private communication (1993) (unpublished).

[23]P. Parnaudeau, J. Carlier, D. Heitz, and E. Lamballais, "Experimental and numerical studies of the flow over a circular cylinder at Reynolds number 3900," Phys. Fluids **20**, 085101 (2008).

[24]L. Ong and J. Wallace, "The velocity field of the turbulent very near wake of a circular cylinder," Exp. Fluids **20**, 441 (1996).

[25]H. C. Lim and S. J. Lee, "Flow control of circular cylinders with longitudinal grooved surfaces," AIAA J. **40**, 2027 (2002).

[26]C. Norberg, "Effects of Reynolds number and a low-intensity free stream turbulence on the flow around a circular cylinder," Chalmers Univ. Goteborg, Sweden, Technol. Publ. **87**, 1–55 (1987).

[27]A. L. Dmitry, I. S. Ertesvag, and K. E. Rian, "Large-eddy simulation of the flow over a circular cylinder at Reynolds number 3900 using the OpenFOAM toolbox," Flow Turbul. Combust. **89**, 491 (2012).

[28]S. Wornom, H. Ouvrard, M. V. Salvetti, B. Koobus, and A. Dervieux, "Variational multiscale large-eddy simulations of the flow past a circular cylinder: Reynolds number effects," Comput. Fluids **47**, 44 (2011).

[29]F. Tremblay, M. Manhart, and R. Friedrich, *LES of Flow Around a Circular Cylinder at a Subcritical Reynolds Number With Cartesian Grids* (Springer, 2004).

[30]E. Salvatici and M. V. Salvetti, "Large eddy simulations of the flow around a circular cylinder: Effects of grid resolution and subgrid scale modeling," Wind Struct. **6**, 419 (2003).

Published under an exclusive license by AIP Publishing

[31]J. Son and T. Hanratty, "Velocity gradients at the wall for flow around a cylinder at Reynolds numbers from 5×10^3 to 10^5," J. Fluid Mech. **35**, 353 (1969).
[32]C. Norberg, "An experimental investigation of the flow around a circular cylinder: Influence of aspect ratio," J. Fluid Mech. **258**, 287 (1994).
[33]M. Arie, M. Kiya, M. Moriya, and H. Mori, "Pressure fluctuations on the surface of two circular cylinders in tandem arrangement," ASME J. Fluids Eng. **105**, 161 (1983).
[34]B. Cantwell and D. Coles, "An experimental study of entrainment and transport in the turbulent near wake of a circular cylinder," J. Fluid Mech. **136**, 321 (1983).
[35]B. E. Lee and S. Basu, "Nonintrusive measurements of the boundary layer developing on a single and two circular cylinders," Exp. Fluids **23**, 187 (1997).
[36]G. S. West and C. J. Apelt, "Measurements of fluctuating pressures and forces on a circular cylinder in the Reynolds number range 10^4 to 2.5×10^5," J. Fluid Struct. **7**, 227 (1993).
[37]C. Norberg, "Fluctuating lift on a circular cylinder: Review and new measurements," J. Fluid Struct. **17**, 57 (2003).
[38]M. A. Prsic, M. Ong, B. Pettersen, and D. Myrhaug, "Large eddy simulations of flow around a smooth circular cylinder in a uniform current in the subcritical flow regime," Ocean Eng. **77**, 61 (2014).
[39]F. Bouak and J. Lemay, "Passive control of the aerodynamic forces acting on a circular cylinder," Exp. Therm. Fluid Sci. **16**, 112 (1998).
[40]J. DuarteRibeiro, "Fluctuating lift and its spanwise correlation on a circular cylinder in a smooth and in a turbulent flow: A critical review," J. Wind Eng. Ind. Aerodyn. **40**, 179 (1992).
[41]J. S. Humphreys, "On a circular cylinder in a steady wind at transition Reynolds numbers," J. Fluid Mech. **9**, 603 (1960).
[42]W. Ma, Q. Liu, J. Macdonald, X. Yan, and Y. Zheng, "The effect of surface roughness on aerodynamic forces and vibrations for a circular cylinder in the critical Reynolds number range," J. Wind Eng. Ind. Aerodyn. **187**, 61 (2019).
[43]H. Weller, "Controlling the computational modes of the arbitrarily structured C grid," Mon. Weather Rev. **140**, 3220 (2012).
[44]Y. Cao and T. Tamura, "Large-eddy simulations of flow past a square cylinder using structured and unstructured grids," Comput. Fluids **137**, 36 (2016).
[45]T. Mukha, S. Rezaeiravesh, and M. Liefvendahl, "A library for wall-modelled large-eddy simulation based on OpenFOAM technology," Comput. Phys. Commun. **239**, 204 (2019).

Published under an exclusive license by AIP Publishing